How to cite: *Angew. Chem. Int. Ed.* **2024**, *63*, e202413058
doi.org/10.1002/anie.202413058

*Operando Characterization for Batteries*

# Influence of Chloride and Electrolyte Stability on Passivation Layer Evolution at the Negative Electrode of Mg Batteries Revealed by operando EQCM-D

*Benjamin W. Schick, Viktor Vanoppen, Matthias Uhl, Matthias Kruck, Sibylle Riedel, Zhirong Zhao-Karger, Erik J. Berg, Xu Hou,* and Timo Jacob**

**Abstract:** Rechargeable magnesium batteries are promising for future energy storage. However, among other challenges, their practical application is hindered by low coulombic efficiencies of magnesium plating and stripping. Fundamental processes such as the formation, structure, and stability of passivation layers and the influence of different electrolyte components on them are still not fully understood. In this work, we gain unique insights into the initial Mg plating and stripping cycles by comparing magnesium bis(trifluoromethanesulfonyl)imide ($Mg(TFSI)_2$)- and magnesium tetrakis(hexafluoroisopropyloxy)borate ($Mg[B(hfip)_4]_2$)-based electrolytes, each with and without $MgCl_2$, on gold electrodes by highly sensitive operando electrochemical quartz crystal microbalance with dissipation monitoring (EQCM–D) applying hydrodynamic spectroscopy. With the stable $Mg[B(hfip)_4]_2$-based electrolytes, highly efficient and interphase-free cycling is possible and passivation layers are attributed to electrolyte contaminants. These are forming and degrading during the so-called initial conditioning process. With the more reactive $Mg(TFSI)_2$-based electrolyte, thick passivation layers with small pores are growing during cycling. We demonstrate that the addition of chloride lowers the amount of passivated Mg deposits in these electrolytes and accelerates the currentless dissolution of the passivation layer. This has a positive effect since we observe the most efficient cycling and uniform deposition when no interphase is present on the electrode.

## Introduction

Due to their high theoretical energy density, higher abundance and lower tendency to form dendrites, rechargeable Mg batteries are an interesting alternative battery chemistry.[1–3] To make use of the high theoretical energy density, Mg metal needs to be used as the negative electrode (also commonly named as anode) of the battery. Therefore, one major challenge is finding an electrolyte that is compatible with the Mg metal and capable of realizing Mg plating and stripping with a coulombic efficiency close to 100 %. To achieve this, the combination of Mg metal and electrolyte must not lead to passivation phenomena or non-uniform Mg deposits.[4,5] Several Mg salts, mostly dissolved in ethers like dimethoxyethane (DME), are investigated to overcome that challenge. Among them, $Mg(TFSI)_2$ as a commercially available salt is widely used as a main component for Mg electrolytes. However, it was found that the single salt $Mg(TFSI)_2$ electrolyte suffers from side reactions due to instability towards Mg which leads to low coulombic efficiencies, passivation phenomena, and low cycling stability.[6–8] In particular, undercoordinated $TFSI^-$ anions might have a higher reactivity towards Mg than bare $TFSI^-$.[6] Furthermore, contaminants like oxygen or water tend to react with Mg to form passivating oxides or hydroxides.[9,10] It is commonly known that the addition of $MgCl_2$ helps to overcome these issues by increasing the coulombic efficiency and reducing the overpotentials for Mg

[*] B. W. Schick, M. Uhl, M. Kruck, Prof. Dr. T. Jacob
Institute of Electrochemistry
Ulm University
Albert-Einstein-Allee 47, 89081 Ulm, Germany
E-mail: timo.jacob@uni-ulm.de

V. Vanoppen, Prof. Dr. E. J. Berg, Dr. X. Hou
Department of Chemistry – Ångström Laboratory, Structural Chemistry
Uppsala University
Lägerhyddsvägen 1, 752 37 Uppsala, Sweden
E-mail: xu.hou@kemi.uu.se

Dr. S. Riedel, Dr. Z. Zhao-Karger, Prof. Dr. T. Jacob
Helmholtz-Institute Ulm (HIU) Electrochemical Energy Storage
Helmholtzstr. 11, 89081 Ulm, Germany

Dr. Z. Zhao-Karger
Institute of Nanotechnology
Karlsruhe Institute of Technology (KIT)
P.O. Box 3640, 76021 Karlsruhe, Germany

Prof. Dr. T. Jacob
Karlsruhe Institute of Technology (KIT)
P.O. Box 3640, 76021 Karlsruhe, Germany

plating and stripping.[5,10–13] At the same time, the addition of chloride is seen as disadvantageous in terms of corrosion of current collector and battery housing made of aluminium and stainless steel.[14] The positive effect of $MgCl_2$ addition has not only been found for $Mg(TFSI)_2$-based electrolytes but also for other Mg electrolytes.[15,16] Multiple studies have attempted to explain these improvements but the reasons are still under debate.[5,17] One explanation is the preferential adsorption of chloride on the Mg surface, thereby preventing electrolyte decomposition which would lead to passivation.[10,11,18] Another approach focuses on the complexes in the electrolyte which are active for Mg plating. By that, active chloro-complexes such as $Mg_2Cl_3^+$ were identified.[13,19] The impact of chloride on passivating layers was the subject of speculation by Salama et al. in 2017.[19] It was proposed that the chloride might help to dissolve passivating MgO and $Mg(OH)_2$ layers. To the best of our knowledge, this idea was not pursued further and has not yet been experimentally confirmed. It is challenging to observe such phenomena experimentally as commonly used ex situ techniques, such as X-ray photoelectron spectroscopy, may deliver misleading results as the interface is highly sensitive and can easily be changed during cell disassembly or cleaning of the sample.[4] Therefore, the fundamental processes at the electrode/electrolyte interface and the formation and morphology of interphases and passivation layers are not yet understood, which stresses the need for in-depth research on this topic.[4,7,10,19–22]

A unique and highly sensitive method to gain deeper insights into mass and morphology changes on metal electrodes under operating conditions is the electrochemical quartz crystal microbalance with dissipation monitoring.[23–26] EQCM-D offers the possibility to overcome the lack of understanding of the above-mentioned issues on Mg deposition. In our previous work, the structural evolution of the working electrode within the initial Mg plating and stripping cycles was investigated using a $Mg(TFSI)_2/MgCl_2$-based electrolyte with tetrabutylammonium borohydride ($TBABH_4$) as additive.[27] By applying advanced characterization with EQCM–D-based hydrodynamic spectroscopy, it was shown that a porous interphase or passivation layer is forming during Mg stripping which is slowly dissolving at the open circuit potential (*ocp*). EQCM without consideration of overtones and bandwidths was recently applied in other studies to investigate Mg and Li systems.[28–30]

In the present study, we apply EQCM–D to compare the $Mg(TFSI)_2$-based electrolyte with and without chloride. To understand the influence of the $TFSI^-$ anion on side reaction phenomena and the formation of passivation layers, we also investigate a $Mg[B(hfip)_4]_2$-based electrolyte with and without the addition of $MgCl_2$. The $[B(hfip)_4]^-$ is supposed to be more stable against metallic Mg compared to $TFSI^-$.[31,32] Therefore, it shows a higher coulombic efficiency and an overall better performance.[31,33–35] By comparing the four different electrolytes, we are able to reveal the impact of chloride and the second anion on side reactions, passivation layer formation and stability.

Chloride is identified as an accelerator of passivation layer dissolution, supporting the hypothesis of Salama et al.[19] Furthermore, in the case of the less stable $Mg(TFSI)_2$-based electrolyte, the lack of chloride results in the formation of larger amounts of passivated Mg and therefore in lower coulombic efficiency and a thick and further growing passivation layer with small pores. Besides that, chloride is less important in the $Mg[B(hfip)_4]_2$-based electrolyte, as the anion appears to be intrinsically stable towards Mg, which results in high coulombic efficiencies and mostly passivation layer-free cycling also for the chloride-free electrolyte. Nevertheless, this electrolyte is also less susceptible to contaminants when combined with $MgCl_2$.

## Results and Discussion

To compare the influence of electrolyte composition and the presence of chloride on electrochemical performance, interphase formation, and its stability, the salts $Mg(TFSI)_2$ and $Mg[B(hfip)_4]_2$ were chosen as main components for the electrolytes. Even small amounts of water can have a detrimental effect by reacting with Mg to form passivating MgO and $Mg(OH)_2$.[10,36] To exclude the impact of water contamination and enable revealing the influence of the electrolyte components themselves, $TBABH_4$ was added to all electrolytes to scavenge water impurities and prevent a pronounced conditioning process within the first plating and stripping cycles.[16,34,37–39] The four electrolytes which were investigated in this study are 115 mM $Mg(TFSI)_2$ and 15 mM $TBABH_4$ in dimethoxyethane (DME) with and without 115 mM $MgCl_2$, as well as 120 mM $Mg[B(hfip)_4]_2$ and 20 mM $TBABH_4$ in DME with and without 120 mM $MgCl_2$.

In the EQCM–D measurement, electrochemical data is combined with the change in resonance frequency $\Delta f_n$ and in bandwidth $\Delta W_n$ of Au-coated quartz-crystals for the overtone orders $n = 3$–13.

This enables not only measuring the mass changes, which are proportional to the decrease in frequency according to the Sauerbrey equation (Equation S1), but also to obtain detailed information on structures which are forming on the electrode surface (Equations S4–10).[26,27,40–43] The changes in bandwidth, which are different for the respective overtone orders, make this necessary, meaning that the sole description by the Sauerbrey equation is not sufficient for the investigated systems. A detailed description of EQCM–D and its use is given in our previous publications and in the Supporting Information.[27,44]

### $Mg(TFSI)_2$-based Electrolytes

In Figure 1, the electrochemical measurement, as well as the $\Delta f_n$ and $\Delta W_n$ response of the overtone orders 5 and 9 for the initial 5 plating and stripping cycles with a plating current density of $-0.5\ mA\,cm^{-2}$ for 3 min of the chloride-free and the chloride-containing $Mg(TFSI)_2$-based electrolytes are exemplarily shown in comparison to each other. In Figure 1a, the potential profiles of the galvanostatic cycles reveal a similar overall shape. However, the clearly higher overpotential of around −0.4 V *vs.* Mg for the formation of

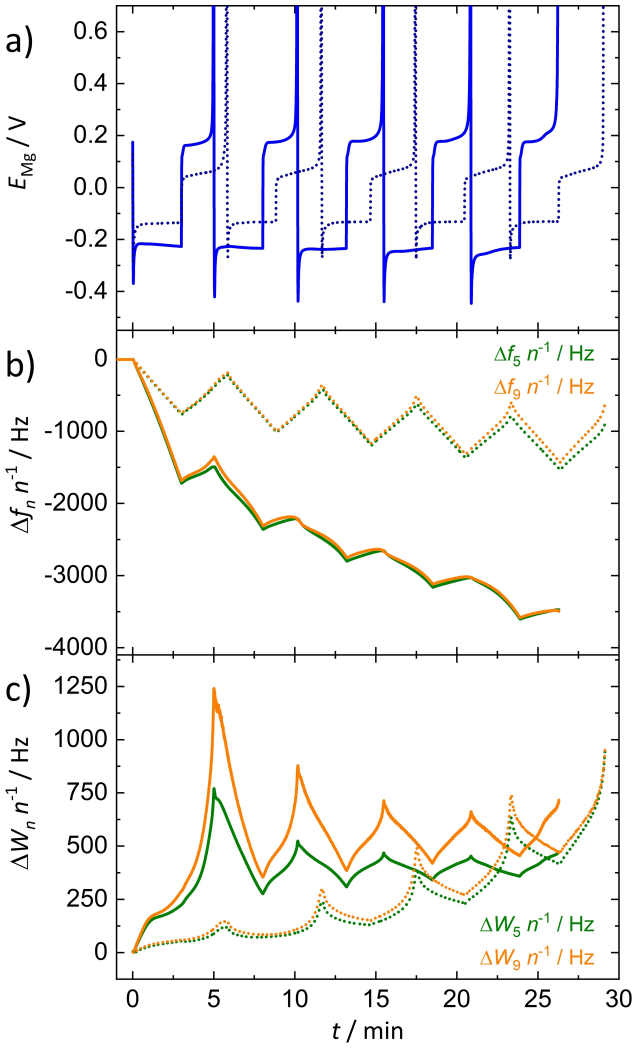


***Figure 1.*** Initial 5 galvanostatic plating and stripping cycles on an Au-coated quartz crystal with a current density of −0.5 mA cm$^{-2}$ for 3 min, followed by a dissolution with 0.5 mA cm$^{-2}$ and a cut-off potential of 1.5 V *vs.* Mg. The continuous lines show the data for the chloride-free $Mg(TFSI)_2$-based electrolyte and the dotted lines the variant with chloride. a) shows the potential $E_{Mg}$ *vs.* time *t*, b) $\Delta f_n\, n^{-1}$ vs. time for overtone orders 5 (green) and 9 (orange), and c) $\Delta W_n\, n^{-1}$ *vs.* time for the respective overtone orders.

the first nuclei in the chloride-free electrolyte demonstrates a larger barrier for their formation. In addition, the overpotentials for plating and stripping are each about 100 mV higher than for the chloride-containing electrolyte and are slightly increasing during the initial cycles.[16] Furthermore, the coulombic efficiency is much lower than for the chloride-containing electrolyte (Figure 1a and 2a), which is in agreement with reports from literature.[11,16,45] In the frequency and bandwidth responses, there are significant differences caused by the presence of chloride (Figure 1b/c). The reversibility in frequency is only around 20 % in the chloride-free electrolyte (Figure 1b and S1), which is very low compared to the coulombic efficiency and as well to the chloride-containing variant.

This means that a relatively thick layer remains on the electrode surface after Mg stripping. As our EQCM–D study does not reveal a pronounced beneficial effect of the formed layer on electrochemical performance, we name it the passivation layer as being suggested for systems with anode-free cells.[46] At the same time, the formed layer still enables further Mg plating in our experiments. The EQCM–D technique does not provide direct information on the chemical composition. Most probably the layer consists of Mg deposits which are housed by a layer composed of reaction products. Traces of reaction products have been found by Horia et al.[16] The negative effect of the layer is more pronounced when thicker layers of Mg are deposited.[16] We avoid the terminology of solid electrolyte interphase (SEI) which would imply a positive and desired process of interphase formation as known from lithium-ion batteries.

Another obvious difference between the chloride-containing and the chloride-free $Mg(TFSI)_2$-based electrolyte is the frequency change during the initial Mg deposition step. To compare the mass change per mole of electrons (*mpe*), $\Delta f_5$ of the first deposition step was plotted *vs.* the transferred charge density $\sigma$ for the four different electrolytes with a deposition current of 1 mA cm$^{-2}$, which is shown in Figure 2b. By combining the Sauerbrey equation with Faraday's law (Equation S2), *mpe* values can be calculated from the slope.[47] The colored area in Figure 2b indicates the section used for fitting the *mpe* values, which has been chosen due to the linear relation of frequency and charge, enabling the application of the Sauerbrey equation. The $Mg(TFSI)_2$-based electrolyte without chloride stands out in this comparison as it shows a clearly higher mass change per electron compared to the other three electrolytes. The others show an *mpe* value which is around the expected molar mass for Mg ($mpe = 12.15$ g mol$^{-1}$). Small deviations could result from marginal changes in the electrochemically active surface area due to the position of the sealing ring during cell assembly.

Interestingly, the frequency change per charge is higher at the beginning of deposition for all four electrolytes, which could be attributed to the formation of the first deposits. This is connected to a roughening of the surface with trapped liquid leading to a higher mass change, which is in agreement with an increasing bandwidth at the beginning of deposition.

The overall higher *mpe* value in the chloride-free $Mg(TFSI)_2$-system could be attributed to side reactions of Mg with the electrolyte as the reaction products, which at least partially remain on the surface, have a higher mass than pure Mg (Figure S2). When repeating the measurement, we found that small differences in coulombic efficiency are connected to relatively large differences in frequency (Figure S3). For instance, a difference in coulombic efficiency of 4 % led to a relative increase in frequency change of about 15 to 20 %. This cannot completely be explained by the higher mass of reaction products. A further explanation is the non-uniform deposition of Mg in this system. The formation of complex morphologies, which might be attributed to the presence of passivation films,

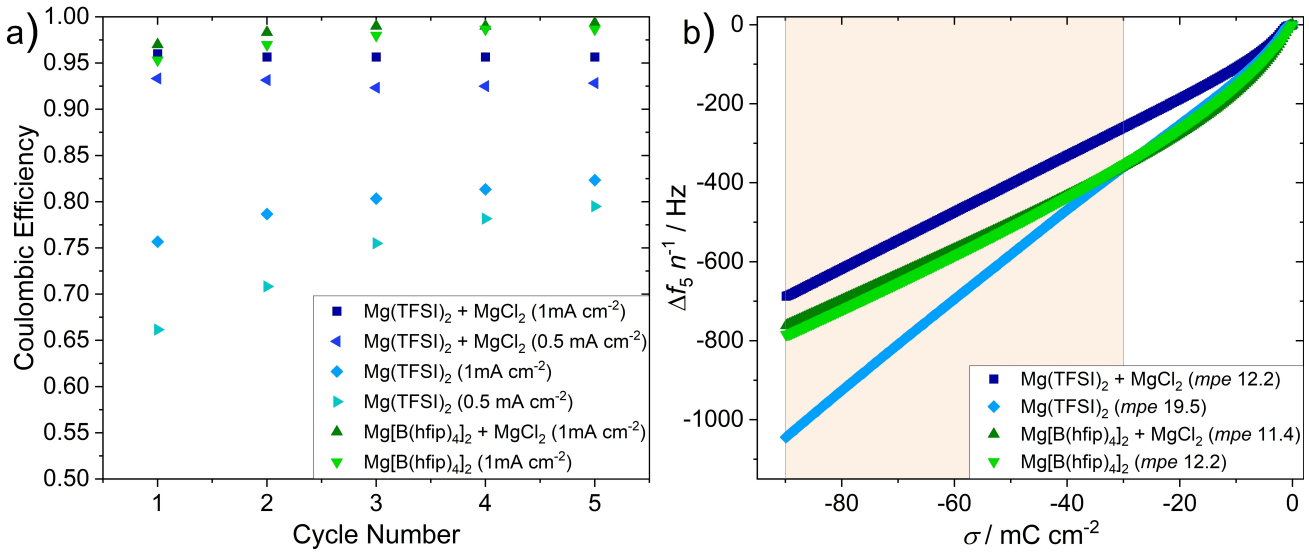


***Figure 2.*** a) Coulombic efficiency *vs.* cycle number for the initial 5 plating and stripping cycles for the different electrolytes. All of them contain $TBABH_4$ as additive. For the $Mg(TFSI)_2/MgCl_2$-based electrolyte with 1 mA cm$^{-2}$, the first cycles after layer removal at high potentials are shown; b) $\Delta f_5\, n^{-1}$ *vs.* charge density $\sigma$ for the initial Mg deposition step at a deposition current density of −1 mA cm$^{-2}$ for the four electrolytes.

could contain small pores which contribute to the Sauerbrey mass as trapped liquid.[16,42,48,49] This is in agreement with studies of an $Mg(TFSI)_2$-based electrolyte by Bachhav et al.[50] and Yoo et al.,[18] and these structures were also observed for other electrolytes where coulombic efficiency was reduced, for example due to contaminants in the electrolyte.[51]

To obtain deeper information on the structure of the formed layer, all $\Delta f_n$ and $\Delta W_n$ for the overtone orders $n = 3$–13 are included by plotting the corresponding hydrodynamic spectra (Figure 3a) analogue to how it was done in our previous work.[27] In these spectra, $\Delta f_n$ and $\Delta W_n$ are plotted *vs.* penetration depth $\delta$ which is a function of overtone order. The penetration depth of the oscillation into the electrolyte becomes smaller as the overtone order increases and is also a function of viscosity $\eta_l$ and density $\rho_l$ of the liquid (equation 1).[26,41]

$$\delta = \left(\frac{\eta_l}{\pi n f_0 \rho_l}\right)^{\frac{1}{2}} \quad (1)$$

In the simplest case of a flat surface, the changes in frequency would be proportional to the penetration depth, which is described by the Kanazawa equation (Equation S3). But the observed layers are not flat as indicated by the changes in bandwidth in Figure 1c. Furthermore, the surface layer is assumed to be stiff as the plated metallic Mg is rigidly attached to the Au surface.

Hydrodynamic spectroscopy is able to describe these stiff but not flat surface layers on the quartz crystal.[26] For the hydrodynamic spectra in Figure 3, galvanostatic cycles with a current density of 1 mA cm$^{-2}$ were selected, which show the same trend but less pronounced bandwidth changes compared to measurements with lower current densities, which means a more uniform and less rough deposition and dissolution is taking place. The reason for this is probably the formation of more nuclei over the whole surface due to the more negative potentials at the beginning of deposition and less time for side reactions during deposition. During the first Mg deposition step in the chloride-free electrolyte, bandwidths only slightly increase. During dissolution, the bandwidths increase more significantly and similarly to how it was observed in the chloride-containing system.[27] But for the chloride-free electrolyte, however, no "hump" is observed in the spectrum but the deviation of $\Delta W_n$ from the initial values after immersion in the liquid increases with decreasing penetration depth. For both $Mg(TFSI)_2$-based electrolytes the hydrodynamic model for the uniform porous layer is applied (Equations S4–S8). In these equations, the surface is assumed to be completely covered with deposits as it was observed by naked eye and SEM, which allows to apply a simplified equation without including the surface coverage as variable. The lateral parameter $\xi$ and the thickness of the porous layer $h$ were extracted by fitting the data points of the bandwidth part in Figure 3c to the equation of the homogeneous porous layer model (Equation S5). The extracted parameters from the bandwidth fit were then used to calculate the expected changes in frequency by applying them to the equation for the frequency part (Equation S4). They reflect the contribution of the porous layer (green double arrow). The mass of the dense Sauerbrey layer $\Delta m_{\text{dense+trapped liquid}}$ (exemplarily indicated by the blue double arrow in Fig 3a) was then determined by calculating the offset between the experimental data points for the frequencies and the contribution of the porous layer extracted from the model.

If these models are applied for the chloride-free electrolyte (Figures 3a and S4), the hump becomes visible at lower penetration depths which are not experimentally accessible with the measured overtone orders in this electrolyte at

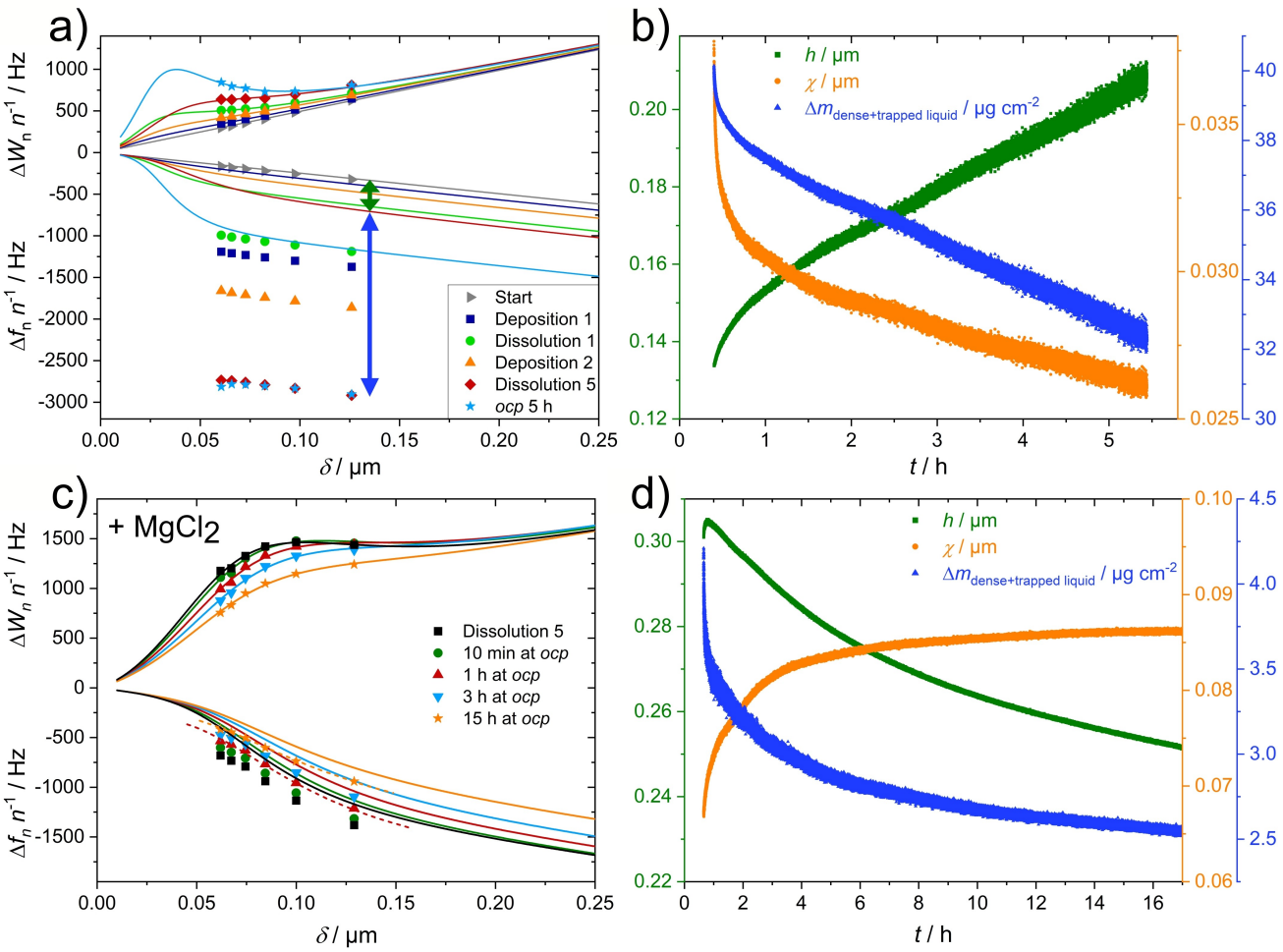


***Figure 3.*** a) Selected hydrodynamic spectra for the $Mg(TFSI)_2$-based electrolyte during 5 plating and stripping cycles at $\pm 1$ mA cm$^{-2}$ for 90 s and after 5 h at *ocp*. The green double arrow marks the contributions of the porous layer to the frequency change and the blue double arrow the contribution of the dense layer, exemplarily for dissolution 5; b) Corresponding extracted parameters for the currentless passivation layer dissolution process after 5 plating and stripping cycles with $h$ (green), $\xi$ (orange) and $\Delta m_{\text{dense+trapped liquid}}$ (blue).; c) Hydrodynamic spectra for the $Mg(TFSI)_2/MgCl_2$-based electrolyte after 5 plating and stripping cycles at $\pm 500$ µA cm$^{-2}$ for 3 min (black) and after selected times at *ocp*, 10 min (green), 1 h (red), 3 h (blue) and 15 h (orange) with the corresponding fits of the uniform porous layer model; d) Corresponding extracted parameters for the currentless passivation layer dissolution process after 5 plating and stripping cycles with $h$ (green), $\xi$ (orange) and $\Delta m_{\text{dense+trapped liquid}}$ (blue).

room temperature. The hump at a penetration depth of about 0.03 µm means a lower lateral parameter $\xi$, which is connected to a smaller pore size.[41] Hereby, the pore size is about 3 times lower in the chloride-free electrolyte compared to the chloride-containing one. The much lower reversibility in frequency, which can also be seen in the hydrodynamic spectra, could be explained by a large amount of trapped liquid.[42] In the hydrodynamic spectra, the overall frequency change is the sum of the contribution of the porous layer and the dense layer. The latter is also called the Sauerbrey layer as its mass can be calculated by the Sauerbrey equation. As described, the pores of the passivation layer after Mg dissolution are very small. This could mean that liquid is trapped in the lower part of the passivation layer and behaves like a dense layer, thereby contributing to the Sauerbrey mass.[42] Summarizing, the remaining passivation layer is thicker and has smaller pores than the layer in the chloride-containing electrolyte.

When Mg is deposited in the second cycle for the chloride-free electrolyte, the bandwidths decrease, which can be explained by filling the pores, decreasing the thickness of the porous layer, analogue to the chloride-containing system (Figure S5).[27] In the chloride-containing system, the frequency change per deposition step is increasing during the initial cycles, which was explained by the filling of the pores which no longer contribute to the porous layer but to the Sauerbrey mass.[27] The opposite is observed in the chloride-free case (Figure 1b). The change in frequency is the highest in the first deposition step. Then it gets lower from cycle to cycle. Again, an explanation is the consideration of the pores. In this case, the trapped liquid in small pores, which already contributes to the Sauerbrey mass in advance, is exchanged by Mg. By that, only minor frequency

changes are observed. The small pores are also visible in ex situ scanning electron microscopy (SEM) images (Figures S6 and S7) although these results have to be taken with caution as the layer is very sensitive to contact with air and even damaged in the electron beam (Figure S8). This limits the meaningfulness of ex situ measurements with such passivation layers in general.

### *Currentless Passivation Layer Dissolution in $Mg(TFSI)_2$-based Electrolytes*

For Mg, which is deposited from a $Mg(TFSI)_2/MgCl_2$-based electrolyte, the frequencies and bandwidths are highly stable at *ocp* (Figures S9 and S10), showing that the pure and flat plated Mg is stable in this electrolyte. But for the same electrolyte, it was already shown that the passivation layer, which forms during cycling, is somehow unstable at *ocp*.[27] To follow the currentless dissolution process of the passivation layer via hydrodynamic spectroscopy and enable tracking of changes in porous layer thickness and dense layer mass, cycling was stopped after 5 cycles and potential was held at *ocp* for 15 h.

Figure 3 shows some selected spectra (Figure 3c) and the extracted parameters *vs.* time (Figure 3d). In Figure 3d, bandwidths decrease and frequencies increase for all overtone orders. The extracted parameters reveal a decrease in porous layer thickness as well as in the mass of the dense layer, indicating that pores grow in the dense part of the layer and the porous part dissolves as well. With the progressing decrease in thickness of the porous layer, dissolution slows down, most probably due to the smaller surface area which lowers the dissolution rate. The behavior of the formed passivation layer is clearly different in the chloride-free system (Figure 3a). Bandwidths increase during *ocp* time and frequencies are rather constant, as shown in Figure 3a and S11. Especially for low penetration depths, the bandwidth increases which indicates the growth of the porous layer (Figure 3b). By applying the porous layer model, a growth of the porous layer and a simultaneous decrease in mass of the dense layer is the result, keeping the sum of both constant. This means that the growth of pores occurs but the passivation layer is not completely dissolving, retaining a residue of the passivation layer which keeps a constant thickness.

The decrease in the lateral parameter $\xi$ is a further sign that small pores in the Sauerbrey layer are growing which afterwards contribute to the porous layer, lowering its average pore size. Hydrodynamic spectroscopy is applied by assuming a rigid layer on the electrode. This assumption is questionable in the case of the appearing thick and porous passivation layer in the chloride-free system. The frequency for the low penetration depths decreases slightly, which reveals a viscoelastic contribution to the frequency and bandwidth response, as already observed in another system with a porous layer.[42] That makes sense because the growth of pores leads to a loss of structural stability as there is less of the rigid backbone and more of the liquid inside the pores.

Nonetheless, pure viscoelastic modeling (Figure S12) did not result in a good fit, because the passivation layer is most probably a mixture of the stiff porous layer and some viscoelastic contributions due to mechanical instability. The fact that the overall passivation layer thickness stays mostly constant in the chloride-free case demonstrates that the chloride accelerates passivation layer dissolution, as hypothesized by Salama et al.[19] The results and differences in relation to the comparison between the chloride-containing and the chloride-free $Mg(TFSI)_2$ electrolyte are visualized in Figure 4. From these measurements, it is difficult to draw conclusions about the mechanism of how exactly chloride acts at the interface. However, it is likely that the protection of the Mg surface from side reactions is due to the adsorption of chloride ions, which probably also dissolve the reaction products such as MgO.

In both cases the passivation layers are removed at high potentials (Figure S13) and form again after removal, indicating that the electrolyte itself is unstable or - less likely - has a high concentration of impurities.[27] In the chloride-free system, the passivation layer thickness is progressively growing during cycling. No dynamic equilibrium between dissolution and formation is established in the chloride-free variant.[27] This is at least the case for the initial cycles when the thicknesses of the deposited layers can still be measured by EQCM–D. To summarize, this means that the deposited Mg is protected from the unstable electrolyte and passivation layer dissolution is accelerated in the presence of chloride.

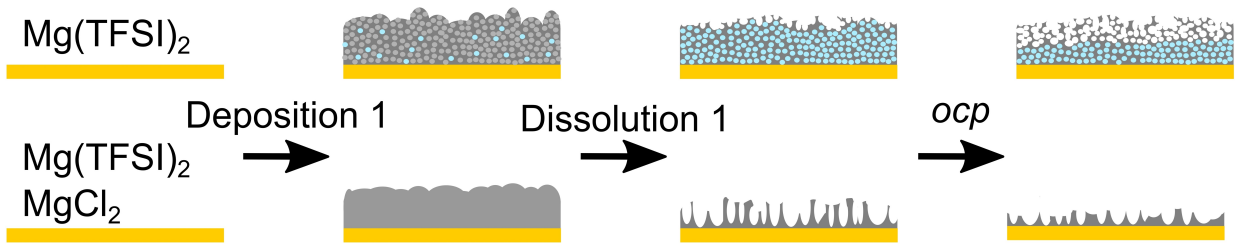


***Figure 4.*** Comparative visualization of the passivation layer formation and dissolution at *ocp* between the $Mg(TFSI)_2$ and the $Mg(TFSI)_2/MgCl_2$-based electrolyte. The blue parts represent the trapped liquid which contributes to the dense layer.

### *Mg[B(hfip)$_4$]$_2$-based Electrolytes*

To compare the passivation layer formation and its stability of Mg(TFSI)$_2$-based electrolytes with more stable electrolytes, Mg[B(hfip)$_4$]$_2$ was chosen as salt to prepare again a $MgCl_2$-containing variant and a chloride-free one.[52,53] Mg[B(hfip)$_4$]$_2$ is expected to be mostly stable against Mg as shown in previous studies.[31–33] The potential profiles of the 1$^{st}$ and the 20$^{th}$ plating and stripping cycles are shown in Figure 5a for both Mg[B(hfip)$_4$]$_2$-based electrolytes. The overpotentials for deposition and dissolution are lower than for the Mg(TFSI)$_2$-based electrolytes in both cases. The differences between the presence and absence of chloride are small regarding the overpotentials and the coulombic efficiencies (Figure 2a). In both electrolytes, overpotentials are decreasing, and coulombic efficiency is increasing from cycle 1 to 20. This results in a coulombic efficiency close to 100 % and the overpotential for plating is only slightly more than −100 mV in the 20$^{th}$ cycle. Nevertheless, the chloride-free electrolyte exhibits overpotentials which are a little higher and a slightly lower coulombic efficiency.

Figure 5b shows the changes in bandwidth and frequency for the initial 20 cycles with and without the addition of $MgCl_2$ as well as the magnification of cycle 3. High reversibility of frequency and bandwidth is achieved, which is correlated with the high coulombic efficiency. Whereas almost no layer forms in the chloride-containing variant, a more pronounced passivation layer formation is observed in the chloride-free Mg[B(hfip)$_4$]$_2$ electrolyte during the initial cycles. With this electrolyte, bandwidth is increasing and frequency is decreasing during the initial two cycles, which means a roughening of the surface. This indicates that the electrolyte is more susceptible to side reactions, but the changes are still small compared to the Mg(TFSI)$_2$-based electrolytes. After the first few cycles, the formed layer degrades again and both electrolytes show a very similar shape in $\Delta f_n$ and $\Delta W_n$. After 20 cycles, $\Delta f_n$ and $\Delta W_n$ are almost at the initial values, indicating the presence of a mostly bare gold surface, which is in agreement with the stabilization of coulombic efficiency at very high levels, indicating that no side reactions are occurring. The slight deviation in $\Delta f_n$ and $\Delta W_n$ after 20 cycles in comparison with the initial values could be either explained by a slight roughening of the surface or slight changes in electrolyte viscosity (Figure S14). Changes in viscosity due to adjustment of temperature or slow solvent evaporation, which increases viscosity in the residual electrolyte, are the more plausible explanation as small changes are also observed at *ocp* before starting the Mg plating and stripping cycles (Figure S15).

The $\Delta f_n$ and $\Delta W_n$ response within one cycle also shows an interesting shape, similar for both electrolytes but different compared to the Mg(TFSI)$_2$-based ones (Figures 5b and 6b). When plating starts, the bandwidth increases and frequency decreases faster than one would expect when depositing a flat Mg layer. This means that the electrode roughens during the formation of the first deposits.

In the further course of deposition, bandwidth is slightly decreasing again, indicating a flat deposition of a dense Mg layer, also reflected by the *mpe* values which are close to the expected values for Mg (Figure 2b). It has to be mentioned that the overall bandwidth changes during deposition are very low (Figure 6a). By fitting the hydrodynamic spectra to the shallow roughness model and uniform porous layer model, it becomes clear that the bandwidth changes correlate with the roughness of the layer (Figures S16 and S17).[41] During Mg stripping, the surface roughening is more pronounced than during the plating step. Towards the end of Mg stripping, the bandwidth is increasing fast (Figure 6), followed by a rapid drop of the bandwidth towards the initial value during the last moments of Mg dissolution. The behavior is similar to already reported copper plating and

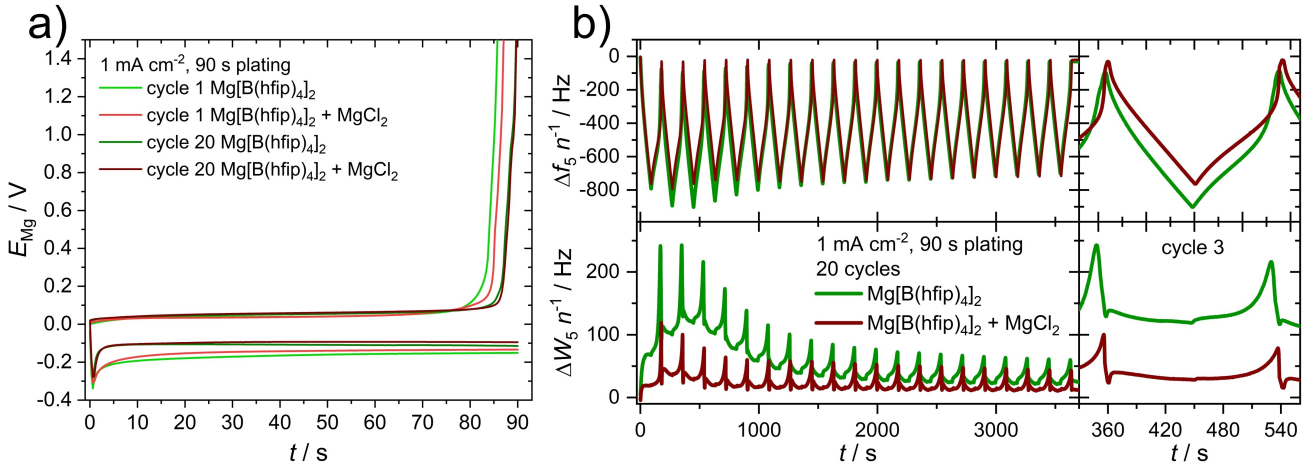


***Figure 5.*** a) Potential profiles for the galvanostatic Mg deposition and dissolution from a Mg[B(hfip)$_4$]$_2$-based (green) and a Mg[B(hfip)$_4$]$_2$/$MgCl_2$-based electrolyte (red) of the 1$^{st}$ and 20$^{th}$ cycle; b) $\Delta f_5\, n^{-1}$ and $\Delta W_5\, n^{-1}$ of the initial 20 galvanostatic plating and stripping cycles on an Au-coated quartz crystal with a current density of 1 mA cm$^{-2}$ for 90 s, followed by a dissolution at 1 mA cm$^{-2}$ with a cut-off potential of 1.5 V *vs.* Mg. The Mg[B(hfip)$_4$]$_2$-based electrolyte is shown in green and the Mg[B(hfip)$_4$]$_2$/$MgCl_2$-based electrolyte in dark red. On the right side, a magnified view of cycle 3 is shown.

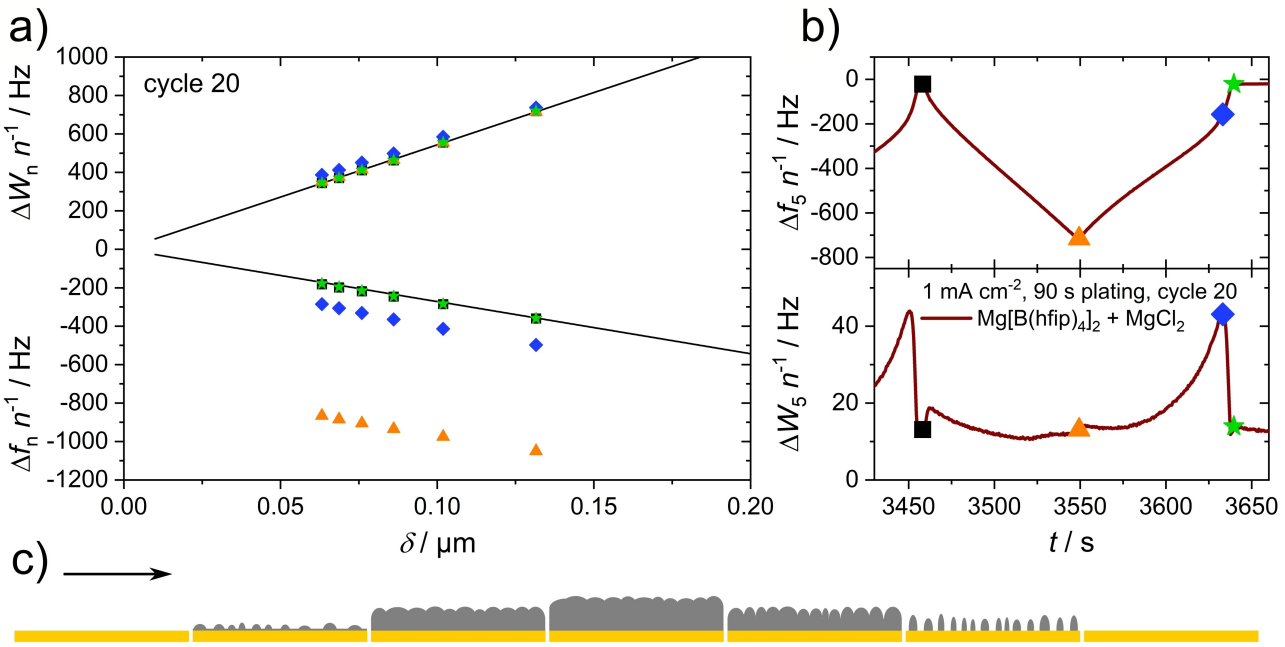


***Figure 6.*** a) Hydrodynamic spectra for selected points during the 20$^{th}$ Mg plating and stripping cycle from the Mg[B(hfip)$_4$]$_2$/MgCl$_2$-based electrolyte. The black line represents the fit to the shallow roughness model in the beginning of the cycle; b) Position of the selected points in the frequency and bandwidth profile; c) Visualization of the changes in Mg deposit morphology in the course of one plating and stripping cycle from a clean Mg[B(hfip)$_4$]$_2$-based electrolyte.

stripping, but the increase of bandwidth at the end of dissolution is more pronounced in the Mg system.[54] The decrease in bandwidth at the very end of Mg dissolution is in strong contrast to the Mg(TFSI)$_2$-based electrolytes, where the stripping step with a cut-off potential of 1.5 V *vs.* Mg ends with a roughening of the surface. In the Mg[B(hfip)$_4$]$_2$ case, the remaining deposits are removed at the very end, leaving behind a bare electrode. For the removal of the last residues of the Mg layer, a higher potential (up to 0.8 V *vs.* Mg) is needed for the Mg stripping to reach the bare electrode (Figure S18). In contrast to that, much higher potentials (>2 V *vs.* Mg) are needed to remove the remaining porous passivated deposits in the Mg(TFSI)$_2$-based systems. A more detailed discussion of the corresponding hydrodynamic spectra and the applied models can be found in the Supporting Information (Figure S16). Slow layer dissolution is also observed in the chloride-free Mg[B(hfip)$_4$]$_2$-based electrolyte at *ocp* (Figure S19). When higher potentials are applied after 5 cycles in the case of the chloride-free Mg[B(hfip)$_4$]$_2$ electrolyte, the remaining passivation layer is removed (Figure S19), comparable to the Mg(TFSI)$_2$-based systems (Figure S13).[27] The cycles after layer removal are characterized by smoother plating and stripping with low bandwidth changes which indicates that the layer can have a negative impact on the uniformity of the Mg deposits. The passivation layer does not form again in consecutive cycles which is in contrast to the Mg(TFSI)$_2$-based electrolytes. This means that the passivation layer is mainly contaminant-induced and the [B(hfip)$_4$]$^-$ anion itself is stable towards Mg. Apparently, solvent decomposition, which is under debate in literature, does not play a significant role in this system.[7] On the other hand, the passivation layer in Mg(TFSI)$_2$-based electrolytes, which forms again and again after removal, is probably caused by instabilities of the electrolyte components themselves or less likely by a very high concentration of contaminants, which were not scavenged by TBABH$_4$.

The changes in electrode structure within one plating and stripping cycle, which shows the same trends in both Mg[B(hfip)$_4$]$_2$-based electrolytes, if they are clean, are visualized in Figure 6c. The comparison between the Mg(TFSI)$_2$-based electrolyte and the Mg[B(hfip)$_4$]$_2$-based electrolyte reveals clear differences between the systems. Whereas the Mg(TFSI)$_2$-based electrolytes show passivation layer formation within the applied potential window, only slight passivation layer formation is observed for the Mg[B(hfip)$_4$]$_2$ electrolytes during the initial cycles which dissolve after some cycles and leave behind a mostly bare electrode.

## Discussion

In literature, there is a variety of studies demonstrating that the presence of chloride improves performance in terms of coulombic efficiency and overpotentials.[10,12,15,55–60] This is also the case if chloride is added to electrolytes with unstable salts, such as Mg(PF$_6$)$_2$, which usually lead to pronounced passivation.[15]

In combination with our study, this can be explained by the protective effect of chloride against side reactions and the removal of passivation layers, which is accelerated by chloride, comparable to the Mg(TFSI)$_2$-based electrolyte in

the presented EQCM–D study. By that, the mixture of $Mg(TFSI)_2$, $MgCl_2$, and $AlCl_3$, which has a high chloride concentration, even showed tolerance towards the addition of water.[57] With scanning electrochemical microscopy (SECM) measurements, it was revealed that $TFSI^-$- and $[B(hfip)_4]^-$-based electrolytes lead to ionically insulating layers, whereby the latter is showing lower resistance.[61] As no water scavenger was used in this study, most probably a thicker passivation layer was formed on the Mg electrode, consisting of MgO and $Mg(OH)_2$, which was not or only slowly dissolved in the absence of chloride. The only electrolyte formulation, where the Mg surface showed low resistance, after being in contact with the electrolyte, was the all-phenyl complex (APC) electrolyte which contains chloride. Again, we propose that the presence of chloride is the decisive factor in the comparison of the three electrolytes. In their study, the highest resistance is observed in the $Mg(TFSI)_2$-based electrolyte as the $TFSI^-$ itself is reactive in addition to the impurity-induced passivation reactions.

Besides our study, the initial cycles of Mg deposition from two other electrolytes were also investigated by EQCM.[28] One of the electrolytes was the chloride-containing APC electrolyte. Fitting to our results, the layer which was formed during cycling with this electrolyte showed a dynamic behavior. Although the coulombic efficiency is only about 95 % after 10 cycles, the layer thickness is decreasing which means that the rate of passivation layer dissolution is higher than that of its formation. The other electrolyte, which did not contain chloride, did not show this dynamic behavior, whereby precise conclusions are difficult as the deposition was not uniform on the entire electrode surface. That implies that the dynamic behavior is also mainly a result of the presence of chloride.

In a study by Horia et al. similar electrolyte formulations to our study were investigated.[16] In the case of a triflate-based electrolyte, performance was improved by the addition of $MgCl_2$. Mg bis(hexamethyldisilazide) $[Mg(HMDS)_2]$ showed no large differences except less pronounced conditioning during the initial cycles, implying that the anion is stable towards metallic Mg.[16,37] By that, the need to introduce chloride for surface protection, besides the impact of impurities, is alleviated and this could explain why the exchange of chloride by bromide still enables reversible Mg deposition in $Mg(HMDS)_2$-based electrolytes.[45,62] It is possible that bromide could also partially adopt the function of chloride. In the studies of Horia et al. and Chinnadurai et al., coulombic efficiency decreased drastically for the $Mg(TFSI)_2$-based systems after a few cycles.[16,45] As the amount of deposited Mg was relatively high compared to our EQCM-D study, most likely a much thicker porous passivation layer was remaining after Mg stripping. This could explain the increasing overpotential for Mg plating and the drastically decreasing coulombic efficiency as the layer probably blocked the reversible Mg deposition.

A recent study by Dlugatch et al. compared the influence of chlorides in $Mg[B(hfip)_4]_2$ electrolytes on the conditioning process and performance.[51] In this case, the lack of impurity-scavenging additives, such as $TBABH_4$, led to a pronounced conditioning process and a positive impact of chloride. This fits perfectly with our results as they show the case of a stable but contaminated electrolyte, where our measurements suggest that chloride is more important as it helps to suppress passivation layer formation and accelerates the dissolution of formed passivation layers.

Kang et al. reported plating and stripping cycles on Mg substrates with different electrolytes.[63] Noteworthy, for the electrolyte that did not contain chloride, the Mg substrate itself was inactive, whereas the Mg substrate was active with the chloride-containing electrolytes. This could be a hint that the native passivation layer on Mg can be removed by chloride as well.

In our opinion, the possible degradation of passivation layers and native films on Mg electrodes and the interface stabilization by chloride should also be taken into account when discussing the beneficial pre-treatment of Mg electrodes with different electrolytes.[64] The main role of borohydrides is most probably scavenging water and other reactive impurities to prevent the formation of the contaminant-induced passivation layers. Furthermore, the decrease in overpotentials and impedance during cycling, which was observed with a $Mg[B(hfip)_4]_2/Mg(BH_4)_2$-based electrolyte, could be attributed to the degradation of passivation layers, which are not forming again in stable electrolytes.[34]

Comparing the results to Li systems, opposite beneficial properties of the interphase layer are revealed. In lithium-ion batteries, the SEI that forms due to the instability of the electrolyte is necessary as it stops the electrolyte from further decomposing but still enables reversible Li plating or insertion. Therefore, a stable SEI is required and SEI dissolution is disadvantageous.[29] In the case of Mg, the opposite is the case as the best performance is reached in the layer-free case.

## Conclusion

To conclude, anion stability, and the presence of contaminants and chloride play a crucial role in the performance of Mg plating and stripping. Passivation layer formation, its structure, and its dissolution as well as the morphology of Mg deposits are strongly affected by these parameters. It was shown that the interphase is rather a passivation layer than a desired SEI in lithium-ion batteries. If the anion is less stable and tends to react with metallic Mg, such as the $TFSI^-$ anion, thick passivation layers with small pores form during cycling. This effect is even enhanced if additional impurities are present in the electrolyte and no moisture-scavenging additives such as $TBABH_4$ are used. The addition of chloride leads to the protection of metallic Mg, which results in a higher coulombic efficiency, a more uniform morphology of deposited Mg, and a thinner layer of passivated Mg. Furthermore, the currentless dissolution of the passivation layer is accelerated in the presence of chloride.

If the anion is stable towards Mg, as in the case of the $[B(hfip)_4]^-$ anion, mostly passivation layer-free plating and stripping is possible. Nevertheless, also in these electrolytes, the protective effect of chloride leads to a lower vulner-

ability to contaminants and thereby less passivation layer formation. The often described but less understood conditioning is dominated by the formation and subsequent degradation of the contaminant-induced passivation layer in stable electrolytes. The fact that the passivation layer resulting from the reaction of contaminants with Mg can be removed at high potentials and does not form again in the subsequent cycles opens up the possibility of preconditioning in order to achieve a more uniform deposition and improve the performance of stable electrolytes.

One promising way for the rational development of electrolytes is finding less corrosive components than chloride, providing the same beneficial properties. Another way is the development of very stable electrolytes with high purity or impurity-scavenging additives which enable efficient cycling also without chloride. The study offers a new perspective on the formation of passivation layers which is influenced by different electrolyte components. The resulting concepts can be extended to other multivalent ion batteries to systematically develop electrolytes with beneficial properties for efficient cycling.

## Acknowledgements

We thank Dr. Maximilian U. Ceblin, Dr. Attila Farkas and Tanja Geng for fruitful and supportive discussions. We thank the German Research Foundation (DFG) for funding under Project ID 390874152 (POLiS Cluster of Excellence), as well as for funding within the priority program SPP 2248 Polymer-based Batteries (Project ID 441209207) and through the individual project with ID 501805371. X.H. acknowledges Energimyndigheten (P2023-00080). X.H., V.V., and E.J.B acknowledge Knut and Alice Wallenberg (KAW) Foundation (Grant 2017.0204), Stiftelsen för Strategisk Forskning (SSF, FFL18- 0269)), and StandUp for Energy for financial support. Open Access funding enabled and organized by Projekt DEAL.

## Conflict of Interest

The authors declare no conflict of interest.

## Data Availability Statement

The data that support the findings of this study are available from the corresponding author upon reasonable request.

**Keywords:** Electrochemistry · EQCM–D · Hydrodynamic Spectroscopy · Magnesium · Mg Battery Electrolyte

[1] J. Muldoon, C. B. Bucur, T. Gregory, *Chem. Rev.* **2014**, *114*, 11683–11720.
[2] R. Deivanayagam, B. J. Ingram, R. Shahbazian-Yassar, *Energy Storage Mater.* **2019**, *21*, 136–153.
[3] J. A. Blázquez, R. R. Maça, O. Leonet, E. Azaceta, A. Mukherjee, Z. Zhao-Karger, Z. Li, A. Kovalevsky, A. Fernández-Barquín, A. R. Mainar, P. Jankowski, L. Rademacher, S. Dey, S. E. Dutton, C. P. Grey, J. Drews, J. Häcker, T. Danner, A. Latz, D. Sotta, M. R. Palacin, J. F. Martin, J. M. G. Lastra, M. Fichtner, S. Kundu, A. Kraytsberg, Y. Ein-Eli, M. Noked, D. Aurbach, *Energy Environ. Sci.* **2023**, *16*, 1964–1981.
[4] Y. Sun, F. Ai, Y. C. Lu, *Small* **2022**, *18*, 2200009.
[5] J. D. Forero-Saboya, D. S. Tchitchekova, P. Johansson, M. R. Palacín, A. Ponrouch, *Adv. Mater. Interfaces* **2022**, *9*, 2101578.
[6] V. Prabhakaran, G. Agarwal, J. D. Howard, S. Wi, V. Shutthanandan, D. T. Nguyen, L. Soule, G. E. Johnson, Y. S. Liu, F. Yang, X. Feng, J. Guo, K. Hankins, L. A. Curtiss, K. T. Mueller, R. S. Assary, V. Murugesan, *ACS Appl. Mater. Interfaces* **2023**, *15*, 7518–7528.
[7] W. Zhao, Y. Liu, X. Zhao, Z. Pan, J. Chen, S. Zheng, L. Qu, X. Yang, *Chem. Eur. J.* **2023**, *29*, e202203334.
[8] Z. Liang, C. Ban, *Angew. Chem. Int. Ed.* **2021**, *60*, 11036–11047.
[9] R. Attias, M. Salama, B. Hirsch, Y. Goffer, D. Aurbach, *Joule* **2019**, *3*, 27–52.
[10] J. G. Connell, B. Genorio, P. P. Lopes, D. Strmcnik, V. R. Stamenkovic, N. M. Markovic, *Chem. Mater.* **2016**, *28*, 8268–8277.
[11] I. Shterenberg, M. Salama, H. D. Yoo, Y. Gofer, J.-B. Park, Y.-K. Sun, D. Aurbach, *J. Electrochem. Soc.* **2015**, *162*, A7118–A7128.
[12] D. T. Nguyen, A. Y. S. Eng, M. F. Ng, V. Kumar, Z. Sofer, A. D. Handoko, G. S. Subramanian, Z. W. Seh, *Cell Reports Phys. Sci.* **2020**, *1*, 100265.
[13] N. Sa, B. Pan, A. Saha-Shah, A. A. Hubaud, J. T. Vaughey, L. A. Baker, C. Liao, A. K. Burrell, *ACS Appl. Mater. Interfaces* **2016**, *8*, 16002–16008.
[14] J. Muldoon, C. B. Bucur, A. G. Oliver, J. Zajicek, G. D. Allred, W. C. Boggess, *Energy Environ. Sci.* **2013**, *6*, 482–487.
[15] I. Shterenberg, M. Salama, Y. Gofer, D. Aurbach, *Langmuir* **2017**, *33*, 9472–9478.
[16] R. Horia, D. T. Nguyen, A. Y. S. Eng, Z. W. Seh, *Batteries & Supercaps* **2022**, *5*, e202200011.
[17] H. Zhang, L. Qiao, M. Armand, *Angew. Chem. Int. Ed.* **2022**, *61*, e202214054.
[18] H. D. Yoo, S. D. Han, I. L. Bolotin, G. M. Nolis, R. D. Bayliss, A. K. Burrell, J. T. Vaughey, J. Cabana, *Langmuir* **2017**, *33*, 9398–9406.
[19] M. Salama, I. Shterenberg, L. J. W. Shimon, K. Keinan-Adamsky, M. Afri, Y. Gofer, D. Aurbach, *J. Phys. Chem. C* **2017**, *121*, 24909–24918.
[20] R. Dominko, J. Bitenc, R. Berthelot, M. Gauthier, G. Pagot, V. Di Noto, *J. Power Sources* **2020**, *478*, 229027.
[21] J. Zhang, Z. Chang, Z. Zhang, A. Du, S. Dong, Z. Li, G. Li, G. Cui, *ACS Nano* **2021**, *15*, 15594–15624.
[22] Y. Man, P. Jaumaux, Y. Xu, Y. Fei, X. Mo, G. Wang, X. Zhou, *Sci. Bull.* **2023**, *68*, 1819–1842.
[23] N. Shpigel, M. D. Levi, D. Aurbach, *Energy Storage Mater.* **2019**, *21*, 399–413.
[24] V. Dargel, N. Shpigel, S. Sigalov, P. Nayak, M. D. Levi, L. Daikhin, D. Aurbach, *Nat. Commun.* **2017**, *8*, 1389.
[25] P. Lemaire, T. Dargon, D. Alves Dalla Corte, O. Sel, H. Perrot, J. M. Tarascon, *Anal. Chem.* **2020**, *92*, 13803–13812.
[26] N. Shpigel, M. D. Levi, S. Sigalov, L. Daikhin, D. Aurbach, *Acc. Chem. Res.* **2018**, *51*, 69–79.
[27] B. W. Schick, X. Hou, V. Vanoppen, M. Uhl, M. Kruck, E. J. Berg, T. Jacob, *ChemSusChem* **2023**, *17*, e202301269.
[28] S. Fan, S. Cora, N. Sa, *ACS Appl. Mater. Interfaces* **2022**, *14*, 46635–46645.

[29] P. Sayavong, W. Zhang, S. T. Oyakhire, D. T. Boyle, Y. Chen, S. C. Kim, R. A. Vilá, S. E. Holmes, M. S. Kim, S. F. Bent, Z. Bao, Y. Cui, *J. Am. Chem. Soc.* **2023**, *145*, 12342–12350.
[30] T. Alemu, S. A. Pradanawati, S. C. Chang, P. L. Lin, Y. L. Kuo, Q. T. Pham, C. H. Su, F. M. Wang, *J. Power Sources* **2018**, *400*, 426–433.
[31] X. Xie, N. J. Leon, D. W. Small, E. W. C. Spotte-Smith, C. Liao, K. A. Persson, *J. Phys. Chem. C* **2022**, *126*, 20773–20785.
[32] P. Jankowski, Z. Li, Z. Zhao-Karger, T. Diemant, M. Fichtner, T. Vegge, J. M. G. Lastra, *Energy Storage Mater.* **2022**, *45*, 1133–1143.
[33] Z. Zhao-Karger, M. E. Gil Bardaji, O. Fuhr, M. Fichtner, *J. Mater. Chem. A* **2017**, *5*, 10815–10820.
[34] Z. Li, T. Diemant, Z. Meng, Y. Xiu, A. Reupert, L. Wang, M. Fichtner, Z. Zhao-Karger, *ACS Appl. Mater. Interfaces* **2021**, *13*, 33123–33132.
[35] T. Mandai, H. Naya, H. Masu, *J. Phys. Chem. C* **2023**, *127*, 7987–7997.
[36] J. Zhang, J. Liu, M. Wang, Z. Zhang, Z. Zhou, X. Chen, A. Du, S. Dong, Z. Li, G. Li, G. Cui, *Energy Environ. Sci.* **2023**, *16*, 1111–1124.
[37] R. Horia, D. T. Nguyen, A. Y. S. Eng, Z. W. Seh, *Nano Lett.* **2021**, *21*, 8220–8228.
[38] H. Wang, X. Feng, Y. Chen, Y. S. Liu, K. S. Han, M. Zhou, M. H. Engelhard, V. Murugesan, R. S. Assary, T. L. Liu, W. Henderson, Z. Nie, M. Gu, J. Xiao, C. Wang, K. Persson, D. Mei, J. G. Zhang, K. T. Mueller, J. Guo, K. Zavadil, Y. Shao, J. Liu, *ACS Energy Lett.* **2020**, *5*, 200–206.
[39] Z. Ma, M. Kar, C. Xiao, M. Forsyth, D. R. MacFarlane, *Electrochem. Commun.* **2017**, *78*, 29–32.
[40] G. Sauerbrey, *Z. Phys.* **1959**, *155*, 206–222.
[41] M. D. Levi, N. Shpigel, S. Sigalov, V. Dargel, L. Daikhin, D. Aurbach, *Electrochim. Acta* **2017**, *232*, 271–284.
[42] N. Shpigel, S. Sigalov, F. Malchik, M. D. Levi, O. Girshevitz, R. L. Khalfin, D. Aurbach, *Nat. Commun.* **2019**, *10*, 4394.
[43] J. G. Kanazawa, K. Keiji II. Gordon, *Anal. Chem.* **1985**, *57*, 1771–1772.
[44] V. Vanoppen, D. Johannsmann, X. Hou, J. Sjölund, P. Broqvist, E. J. Berg, *Adv. Sens. Res.* **2024**, *3*, 1–18.
[45] D. Chinnadurai, W. Y. Lieu, S. Kumar, G. Yang, Y. Li, Z. W. Seh, *Nano Lett.* **2023**, *23*, 1564–1572.
[46] J. Xiao, Q. Li, Y. Bi, M. Cai, B. Dunn, T. Glossmann, J. Liu, T. Osaka, R. Sugiura, B. Wu, J. Yang, J. G. Zhang, M. S. Whittingham, *Nat. Energy* **2020**, *5*, 561–568.
[47] D. Aurbach, M. Moshkovich, *J. Electrochem. Soc.* **1998**, *145*, 2629–2639.
[48] R. Attias, B. Dlugatch, O. Blumen, K. Shwartsman, M. Salama, N. Shpigel, D. Sharon, *ACS Appl. Mater. Interfaces* **2022**, *14*, 30952–30961.
[49] A. Kushima, K. P. So, C. Su, P. Bai, N. Kuriyama, T. Maebashi, Y. Fujiwara, M. Z. Bazant, J. Li, *Nano Energy* **2017**, *32*, 271–279.
[50] M. N. Bachhav, N. T. Hahn, K. R. Zavadil, E. G. Nelson, A. J. Crowe, B. M. Bartlett, P.-W. Chu, V. J. Araullo-Peters, E. A. Marquis, *J. Electrochem. Soc.* **2016**, *163*, D645–D650.
[51] B. Dlugatch, J. Drews, R. Attias, B. Gavriel, A. Ambar, T. Danner, A. Latz, D. Aurbach, *J. Electrochem. Soc.* **2023**, *170*, 090542.
[52] Z. Zhao-Karger, R. Liu, W. Dai, Z. Li, T. Diemant, B. P. Vinayan, C. Bonatto Minella, X. Yu, A. Manthiram, R. J. Behm, M. Ruben, M. Fichtner, *ACS Energy Lett.* **2018**, *3*, 2005–2013.
[53] W. Ren, D. Wu, Y. Nuli, D. Zhang, Y. Yang, Y. Wang, J. Yang, J. Wang, *ACS Energy Lett.* **2021**, *6*, 3212–3220.
[54] S. Sigalov, N. Shpigel, M. D. Levi, M. Feldberg, L. Daikhin, D. Aurbach, *Anal. Chem.* **2016**, *88*, 10151–10157.
[55] C. Liao, N. Sa, B. Key, A. K. Burrell, L. Cheng, L. A. Curtiss, J. T. Vaughey, J. J. Woo, L. Hu, B. Pan, Z. Zhang, *J. Mater. Chem. A* **2015**, *3*, 6082–6087.
[56] K. W. Leong, W. Pan, Y. Wang, S. Luo, X. Zhao, D. Y. C. Leung, *ACS Energy Lett.* **2022**, *7*, 2657–2666.
[57] Y. He, Q. Li, L. Yang, C. Yang, D. Xu, *Angew. Chem. Int. Ed.* **2019**, *58*, 7615–7619.
[58] L. Yang, C. Yang, Y. Chen, Z. Pu, Z. Zhang, Y. Jie, X. Zheng, Y. Xiao, S. Jiao, Q. Li, D. Xu, *ACS Appl. Mater. Interfaces* **2021**, *13*, 30712–30721.
[59] M. Cheng, W. Ren, D. Zhang, S. Zhang, Y. Yang, X. Lv, J. Yang, J. Wang, Y. NuLi, *Energy Storage Mater.* **2022**, *51*, 764–776.
[60] T. Pavčnik, M. Lozinšek, K. Pirnat, A. Vizintin, T. Mandai, D. Aurbach, R. Dominko, J. Bitenc, *ACS Appl. Mater. Interfaces* **2022**, *14*, 26766–26774.
[61] C. Santana Santos, M. Romio, Y. Surace, N. Eshraghi, M. Amores, A. Mautner, C. Groher, M. Jahn, E. Ventosa, W. Schuhmann, *Chem. Sci.* **2023**, *14*, 9923–9932.
[62] S. Dongmo, S. Zaubitzer, P. Schüler, S. Krieck, L. Jörissen, M. Wohlfahrt-Mehrens, M. Westerhausen, M. Marinaro, *ChemSusChem* **2020**, *13*, 3530–3538.
[63] S. J. Kang, H. Kim, S. Hwang, M. Jo, M. Jang, C. Park, S. T. Hong, H. Lee, *ACS Appl. Mater. Interfaces* **2019**, *11*, 517–524.
[64] Y. Li, P. Zuo, R. Li, H. Huo, Y. Ma, C. Du, Y. Gao, G. Yin, R. S. Weatherup, *ACS Appl. Mater. Interfaces* **2021**, *13*, 24565–24574.

Manuscript received: July 11, 2024
Accepted manuscript online: November 10, 2024
Version of record online: November 19, 2024